https://doi.org/10.1016/j.cej.2023.147405

Facile Spinning of Tough and Conductive Eutectogel Fibers via Li^+-induced Dense Hydrogen-Bond Networks

Lingtao Fang,[1] Chi Zhang,[2] Wenjiao Ge,[1,5] Mingming Rong,[1] Fan Chen,[1] Zijian Chen,[1] Xiaohui Wang,[5] Zijian Zheng,[1,2,3,4] Qiyao Huang[1,3] *

[1] School of Fashion and Textiles, The Hong Kong Polytechnic University, Hung Hom, Kowloon, Hong Kong SAR, China

[2] Department of Applied Biology and Chemical Technology, Faculty of Science, The Hong Kong Polytechnic University, Hung Hom, Kowloon, Hong Kong SAR, China

[3] Research Institute for Intelligent Wearable Systems (RI-IWEAR), The Hong Kong Polytechnic University, Kowloon, Hong Kong SAR, PR China

[4] Research Institute for Smart Energy (RISE), The Hong Kong Polytechnic University, Kowloon, Hong Kong SAR, China

[5] State Key Laboratory of Pulp and Paper Engineering, South China University of Technology, Guangzhou 510640, China

Corresponding email: qihuang@polyu.edu.hk (Dr. Qiyao Huang)

Abstract

Tough conductive eutectogel fibers synthesized based on deep eutectic solvents (DESs) have attracted increasing attention in fields of flexible/stretchable electronics, due to their promising stretchability, mechanical strength, conductivity, and relatively inexpensive cost. However, it is still challenging to fabricate such high-performance eutectogel fibers in a simple and versatile strategy. Here, we report a facile spinning of tough conductive eutectogel fibers based on one-pot photopolymerization and Li^+-induced toughening effect. This photopolymerization allows the formation of eutectogel into a long fiber format within seconds. The introduction of Li salt into the DESs can regulate the hydrogen bonding interactions, which can significantly promote the construction of a dense interchain hydrogen-bonding network in the eutectogel. Consequently, the spun eutectogel fibers exhibit outstanding Young's modulus (103.8 MPa), high toughness (38 MJ/m^3), promising stretchability (>300%), conductivity (6×10^{-3} S/m), and good thermal stability at high temperature. The mechanical properties of the resultant eutectogel fibers can also be modulated by varying the DESs constituents. We demonstrate the multifunction of the fibers in shape-memory behavior, strain sensing, and recyclability. This facile spinning strategy offers a promising way to develop super-strong and conductive gel fibers as smart materials for diverse flexible and wearable device applications.

Keywords

Deep eutectic solvents; Fiber spinning; Eutectogel; Li^+-induced toughening effect; Hydrogen-bond networks

1. Introduction

Gels are polymer networks that are infiltrated with a large amount of liquid solvent. Their tunable optical transparency, good stretchability, and excellent conductivity have attracted increasing attention from both academia and industry.[1-6] More recently, gels show promising potential as soft ionic conductors for flexible/stretchable wearable electronics, human-machine interfaces, mechanoelectrical conversion and soft robotics.[7-14] Many of these applications made use of hydrogels that are composed of functional polymer networks and highly conductive aqueous solvents. Nevertheless, hydrogels face the problem of dehydration at high temperatures. Though the infiltration with organic solvents or ionic liquids could impart the organogels or ionogels with enhanced thermal stability, these gels possess the risks of liquid leakage and high materials cost.[15-19] Recently, deep eutectic solvents (DESs), a low-melting eutectic liquid consisting of a mixture of hydrogen bond donors (HBDs) and hydrogen bond acceptors (HBAs), have been explored as a new class of ionic conductive liquids.[20, 21] Benefiting from their low volatility, high thermal stability, excellent ionic conductivity (~ 0.1-1 S/m) at room temperature, ease of production, and relatively inexpensive materials cost, DESs have been utilized for the fabrication of gels (e.g., eutectogels), which serve as promising replacements for conventional gels in extreme environments, including high temperature, low humidity, and even outer space.[22-27] Yet, most eutectogels show poor mechanical properties, such as low fracture strength (<1 MPa), Young's modulus (<1 MPa), and toughness (<1 MJ/m^3).[28, 29] As a result, these eutectogels usually find applications where robust mechanical properties are not required.[30-32]

Improving the mechanical properties of eutectogel is of great significance to extend their applicability in soft electronics.[33] One strategy to toughen the eutectogel is to construct a strong and dense hydrogen-bond network in the polymeric matrix, which could be realized by utilizing the abundant HBDs and HBAs in DESs.[34] Fabrication strategies, such as solvent replacement, have been explored to regulate the hydrogen bonding interactions between HBDs and HBAs, leading to the formation of a hydrogen-bonding-rich domain in the polymeric network and thus a superb tough eutectogel.[35, 36] Nevertheless, these methods usually

involve multiple fabrication steps as well as tedious and time-consuming post-preparation treatments, which are practically difficult to be scaled up.

On the other hand, state-of-the-art eutectogels are mostly limited to two-dimensional (2D) films or three-dimensional (3D) bulk gels that are difficult to conformally fit the irregular surfaces and 3D shapes of the human body. Shaping gels materials into one-dimensional (1D) fibers can enable excellent compliance on different complex geometrics, easy integration into conventional textiles, and outstanding permeability that is important for long-term wearing.[37] Although several eutectogel fibers have been explored very recently, their low strength (Young's modulus <1 MPa) yet limits their practical applications.[38, 39] To date, endowing eutectogel fibers with tough mechanical properties in a versatile and facile spinning strategy by using simple materials is still challenging.

In this work, we report a facile and rapid spinning strategy based on one-pot photopolymerization and lithium cation (Li^+)-induced toughening effect to develop tough and conductive eutectogel fibers (Eu-fibers). The photopolymerization of DES occurs during the spinning process, allowing for the formation of long Eu-fibers within seconds. Through the experimental investigation and simulation study, the introduction of Li^+ into DES is revealed to significantly promote the formation of dense interchain hydrogen-bond crosslinks among the polymer networks. Such an interchain hydrogen-bonding network can enhance the mechanical properties of the eutectogels. This Li^+-induced toughening effect also works with different Li salts, leading to the formation of a new series of tough and conductive Eu-fibers. Remarkably, the Eu-fiber shows a 500-fold increase in Young's modulus at room temperature compared to those without the toughening of Li^+, and possess high stretchability (>300% strain), good thermal stability at high temperatures, promising conductivity ($4\sim6 \times 10^{-3}$ S/m), and interestingly, a smart glassy-to-rubbery transition at near-body temperature. Taking these merits, these super-strong Eu-fibers, as a proof of concept, can be integrated into different 3D shapes by weaving and braiding technologies, and can exhibit shape-morphing capability under heat stimulus. We also demonstrate the multifunction of Eu-fibers in strain sensing and

recyclability. The novelty of our approach lies in the development of a simple and efficient spinning strategy based on one-pot photopolymerization. Additionally, the unique properties of Li^+ ions are utilized to facilitate the formation of dense hydrogen bond networks, which serve as crosslinks within the polymer network to enhance the toughness of the eutectogel. To the best of our knowledge, our study is the first to propose the toughening effects in eutectogels resulting from the augmentation of hydrogen bond networks induced by small ions. It is anticipated that such a facile spinning approach coupled with Li^+-induced toughening strategy can provide a practical way for achieving super-strong, stretchable, and conductive gel fibers for the applications in multifunctional wearable sensors and soft robotics.

2. Materials and methods

2.1. Materials

Acrylic acid (AAc, ⩾99%), choline chloride (ChCl, ⩾98%), lithium chloride (LiCl, ⩾98%), lithium bromide (LiBr, ⩾99%), lithium acetate (LiOAc, ⩾99%), bis(trifluoromethylsulfonyl)amine lithium salt (LiTFSI, ⩾99%), 2-hydroxy-4'-(2-hydroxyethoxy)-2-methylpropiophenone (photoinitiator 2959, ⩾98%) were purchased from Aladdin Chemistry Co., Ltd. Sudan I (⩾96%) and Deuterium oxide (D_2O, ⩾99.9%) was purchased from Sigma-Aldrich Chemistry Co., Ltd. All chemicals were used without further purification.

2.2. Preparation of eutectogels based on deep eutectic solvents (DESs)

The eutectogels were fabricated through the photopolymerization of the monomers (i.e., hydrogen bond donors (HBDs) in this work) in the deep eutectic solvents (DESs). Briefly, HBD and hydrogen bond acceptor (HBA) were firstly mixed at a specific proportion (Table S1) and then stirred at 80 ºC until the mixture became a transparent liquid (i.e., DES). After cooling down to room temperature, the DES was mixed with the photoinitiator, Irgacure 2959 (0.1 mol%, relative to the HBD), and then ultrasonicated for 10 min until the photoinitiator was fully dissolved. Subsequently, the photopolymerization of the monomers (i.e., AAc) in the DES

was triggered by the irradiation under a 365 nm UV light with the intensity of 45 W at room temperature for 30 s. To fabricate the Eu-fiber, the solution consisting of DES and photoinitiator was injected into a 1 mm diameter polytetrafluoroethylene (PTFE) tube using a syringe, followed by exposure to a 365 nm UV light (45 W) for the polymerization. Afterward, the Eu-fiber with a diameter around 0.95 mm was obtained by cutting a slit in the PTFE tube with scissors and peeling the tube along the created slit. The diameter of Eu-fiber can be controlled by the size of PTFE tube. For performance comparison, hydrogel fibers with similar components were prepared. In these hydrogel fibers, the molar ratios of HBD, HBAs, and photoinitiator were the same, except for the addition of deionized (DI) water (40 wt%).

2.3. Characterizations

The transmittance of eutectogels with a thickness of 1 mm was measured by ultraviolet-Visible spectrometer (UV-Vis, Cary 300) in the wavelength range of 400-800 nm with scanning interval of 2 nm. The amorphous polymeric network of eutectogel was analysed by an X-ray diffractometer (XRD, Rigaku SmartLab 9 kW, Japan) with a Cu Kα X-ray source. Hydrogen bonding interactions in DESs and eutectogels were characterized by ^{1}H Nuclear Magnetic Resonance (NMR) spectrum (Jeol ECZ500R 500 MHz NMR spectrometer) in D_2O at 25 ºC. The melting points of DESs of the formed eutectogels were characterized by the Simultaneous Thermal Analysis (TGA/DSC3+, Mettler Toledo International Inc., Zurich, Switzerland) at a heating rate of 10 ºC/min under nitrogen atmosphere (50 mL/min). The thermal stabilities of eutectogels and hydrogels were also measured by the TGA/DSC3+. The gels were heated from 30 ºC to 700 ºC at a heating rate of 10 ºC/min under flowing nitrogen (50 mL/min). The glass transition temperatures of eutectogels were measured by Dynamic Mechanical Analysis (DMA, Q800 equipment). A rectangular sample (dimensions: 10 mm × 6.5mm × 1 mm) was tested in a single cantilever beam mode with a frequency of 1 Hz and strain of 0.05 mm when the temperature increased from 25 to 80 °C (heating rate: 5 °C/min).

The tensile properties of the Eu-fibers were measured by a universal testing machine (Instron 5566). The gauge length of Eu-fiber samples for the tests was 30 mm and stretched at a speed

of 100 mm/min. The nominal stress (σ) and strain (ε) were recorded, in which the stress was defined as the tensile force divided by the original cross-section area of the sample, and the strain was defined as the displacement of the cross-head divided by the gauge length of the gel sample. Young's modulus was calculated from the initial slope of the stress-strain curve with a strain below 10% before yielding. Toughness was obtained by the area integral of the stress-strain curve for each sample. Fracture energy (Γ) was calculated from the integral area under the stress-strain curve of fiber with the initial clamp distance (H), and the formula is $\Gamma=H\int\sigma d\varepsilon$. The effective crosslinking density (v_e) was determined with the classical rubber elasticity theory proposed by Flory.[40] The equation is given by is $G \approx RTv_e\Phi^{1/3}$, where, R is the gas constant (R = 8.314 J/(mol·K)), T is the absolute temperature (T = 298.15 K), Φ is the volume fraction (could be roughly determined by polymer weight fraction; for PAAc/ChCl Eu-fiber, $\Phi \approx 0.5$). The modulus, G, is the slope of nominal stress and (λ-λ^{-2}) (λ is the deformation ratio; $\lambda = \varepsilon + 1$). Tensile tests at different temperatures were performed in an oven at a specific temperature. More than three samples were tested for one experiment.

The ionic conductivity (σ) of the gels was obtained by the measurement of the gel's resistance R by the AC impedance measurement and the calculation by the formula $\sigma = L/RS$. Briefly, the gel specimen was sandwiched by two stainless steel foils and connected to an electrochemical working station (CHI660E). AC impedance mode with the frequency sweep from 0.01 to 100,000 Hz and initial voltage of 0 V with 5 mV amplitude was conducted to obtain the resistance R at 0° phase angle. The contact area between the metal foil and the eutectogel (S) and the distance between two foils (L, i.e., the thickness of the gel) were measured for the calculation of ionic conductivity. More than three samples were tested for one experiment. The resistance change of the Eu-fiber in response to the tensile strain was recorded by a Keithley 2400 source meter coupled with a customized stretching motor.

2.4. Simulation study

All density functional theory calculations were performed using ORCA 5.0 package. Geometrical optimization and frequency calculations are conducted with m062x functional[41]

and def2-TZVP basis.[42, 43] Dispersion correction is employed through Grimme's D3 damping function.[44] The binding energy was obtained by $E_{binding} = E(AB) - E(A) - E(B)$. Molecular dynamics simulations were performed in LAMMPS using the COMPASS forcefield.[45, 46] For PAAc/ChCl eutectogel, simulation boxes (28.5 Å in lateral length) contained 2 PAAc polymer chains 50 units long each, 50 Ch^+, and 50 Cl^- corresponding to the molar ratio of each components (AAc : ChCl = 10 : 5) in AAc/ChCl DES system. For PAAc/ChCl/LiCl eutectogel, simulation boxes (28.5 Å in lateral length) contained 2 PAAc polymer chains 50 units long each, 50 Ch^+, 10 Li^+, and 60 Cl^- corresponding to the molar ratio of each components (AAc : ChCl : LiCl = 10 : 5 : 1) in AAc/ChCl/LiCl DES system. For the systems, an initial energy minimization (energy and force tolerances of 10^{-4}) was performed to obtain the ground-state structure. After that, the system was slowly heated from 0 K to room temperature at constant volume over 1 ns using a Nose-Hoover thermostat, with a damping parameter of 80 ps. After that, the system was equilibrated in the constant temperature (298 K), constant pressure (1 bar) (NPT ensemble) for 5 ns before finally being subjected to 5 ns of constant volume, constant temperature dynamics. Radial distribution functions (*g(r)*) were obtained using the visual molecular dynamics (VMD) software.[47] Snapshots of the most probable solvation shells were also sampled from the simulation trajectory using VMD. Coordination numbers *(n(r)*) were calculated from *g(r)* using the equation $n(r) = \sum 4\pi r^2 \rho g(r) \delta r$ (ρ: the number of target ion (Cl^-) per unit volume; r: the distance between target position and given ion (Li^+)).

3. Results and discussion

3.1. Construction of eutectogel fibers (Eu-fibers)

The fabrication of Eu-fibers enabled by one-step photopolymerization is depicted in Figure 1a. Briefly, the Eu-fiber was made by a polymerizable acrylic acid (AAc)-choline chloride ($[(CH_3)_3NCH_2CH_2OH]Cl$, ChCl) DES liquid that was added with lithium chloride (LiCl) in the presence of photo-initiators. In our work, we mixed HBD, i.e., AAc, which also served as the monomer for the construction of the polymer network, with HBAs, i.e., ChCl and LiCl, in different molar ratios (Table S1), to form the transparent liquids of DES (denoted as

AAc/ChCl/LiCl DES) without the addition of other solvents (Figure S1). The selection of polymerizable DES units is guided by several considerations. Firstly, we focus on the suitability of AAc due to its chemical composition, which includes a C=C double bond and carboxyl groups, making it an ideal candidate as a polymerizable monomer and a hydrogen bond donor for DES formation. Secondly, we prioritize the preparation of solvent-free eutectogels to avoid any potential issues related to liquid leakage. Factors such as cost and sustainability are also taken into consideration. Notably, AAc, ChCl, and LiCl are low-cost components, facilitating the sustainable production of DES. By considering these criteria, we selected AAc and ChCl as the constituents of our DES system. A widely accepted principle to demonstrate the successful formation of DES is the reduction of the melting point (T_m) in comparison to its HBD and HBA components.[48] Differential scanning calorimetry (DSC) shows that there was only one endothermic peak corresponding to melting point around -13 ºC for the as-formed AAc/ChCl/LiCl DES liquid, which was much lower than that of AAc (13 ºC), ChCl (305 ºC), and LiCl (605 ºC) (Figure S2). In such a deep eutectic system, Cl^- from both ChCl and LiCl could form hydrogen bonding interactions with the carboxyl groups (-COOH) from AAc (denoted as -COOH···Cl^-),[49, 50] leading to the reduction of the melting point of the mixture and thus the formation of a transparent liquid without a phase separation at the room temperature. After the addition of the photo-initiator, Iragace 2959 (0.1 mol% to AAc), the DES liquid as the spinning solution was injected into a polytetrafluoroethylene (PTFE) tube by a syringe, and then the photopolymerization of AAc in the solution was initiated under ultra-violate (UV) light exposure. A eutectogel fiber (denoted as PAAc/ChCl/LiCl Eu-fiber) could be eventually formed in the tube within seconds, which was then extracted and collected after the photo-curing. Owing to the homogeneous and amorphous gel system (Figure S3a) that was composed of dense hydrogen bonds between polymer chains (denoted as O-H···O=C), the as-formed Eu-fiber was imparted with high transparency (Figure S3b). Benefiting from the ease of preparation for the spinning solution and the fast polymerization rate, long fibers could be easily and quickly manufactured. As proof of concept, we demonstrated a 2 m long PAAc/ChCl/LiCl Eu-fiber that was formed within only 30 seconds (inset in Figure 1a).

In such a three-component AAc/ChCl/LiCl DES system, the introduction of LiCl led to a dramatic enhancement in the mechanical properties of the resultant eutectogels. While two-component PAAc/ChCl eutectogel was soft but weak and PAAc/LiCl was rather rigid (Figure S4), PAAc/ChCl/LiCl Eu-fibers possessed outstanding mechanical strength with remained excellent stretchability (Figure 1b). The breaking stress, Young's Modulus, and toughness of the PAAc/ChCl/LiCl Eu-fiber reached 17.3 MPa, 103 MPa, and 38 MJ/m^3, respectively, which showed 30-fold, 500-fold, and 30-fold higher than those of PAAc/ChCl Eu-fiber without the addition of LiCl. Meanwhile, PAAc/ChCl/LiCl Eu-fiber was still able to be stretched up to 367% (Figure 1b). The surface PAAc/ChCl/LiCl Eu-fiber was smooth and compact along the axial direction, which contributed to the improvements in mechanical properties, and the energy-dispersive X-ray spectroscopy (EDS) mapping revealed a uniform dispersion of chloride ions, suggesting that the distribution of LiCl within the fiber was also uniform, without any visible signs of aggregation (Figure S5). Importantly, the newly developed PAAc/ChCl/LiCl Eu-fibers also outperformed the hydrogel fibers (denoted as Hy-fibers) that were made with the same ratios of AAc, ChCl, and LiCl in terms of their mechanical properties (breaking stress and strain, toughness, Young's modulus, and fracture energy) and thermal stability on the whole. For example, the Young's modulus and toughness of PAAc/ChCl/LiCl Eu-fibers respectively demonstrated 340-fold and 690-fold improvement compared to those of PAAc/ChCl/LiCl Hy-fibers (Table S2). To the best of our knowledge, PAAc/ChCl/LiCl Eu-fiber demonstrated the best mechanical performance among the reported eutectogels (Figure 1c and Table S3).[51-55] Through the confirmation with thermogravimetric analysis (TGA), PAAc/ChCl/LiCl Eu-fiber lost only 4% of its weight when the temperature reached 270 °C, while PAAc/ChCl/LiCl Hy-fiber lost more than 20% of their weight (Figure S6). Such mechanical and thermal enhancements of Eu-fibers could be ascribed to the restrained polymer chains that were caused by dense hydrogen bonds and intermolecular entanglements, especially within a solvent-free matrix of eutectogel (Figure 1a).[56] Therefore, Eu-fibers can function as promising candidates of super-strong, thermally stable, and stretchable ionic conductive fibers. As a proof-of-concept demonstration, the super-strong Eu-fiber could lift a 1 kg weight (Figure 1d), and could be braided, knotted, and even woven into various complex 3D geometrics without breaking

(Figure 1e-g), exhibiting its ability to bear large loading and persistent mechanical deformations.

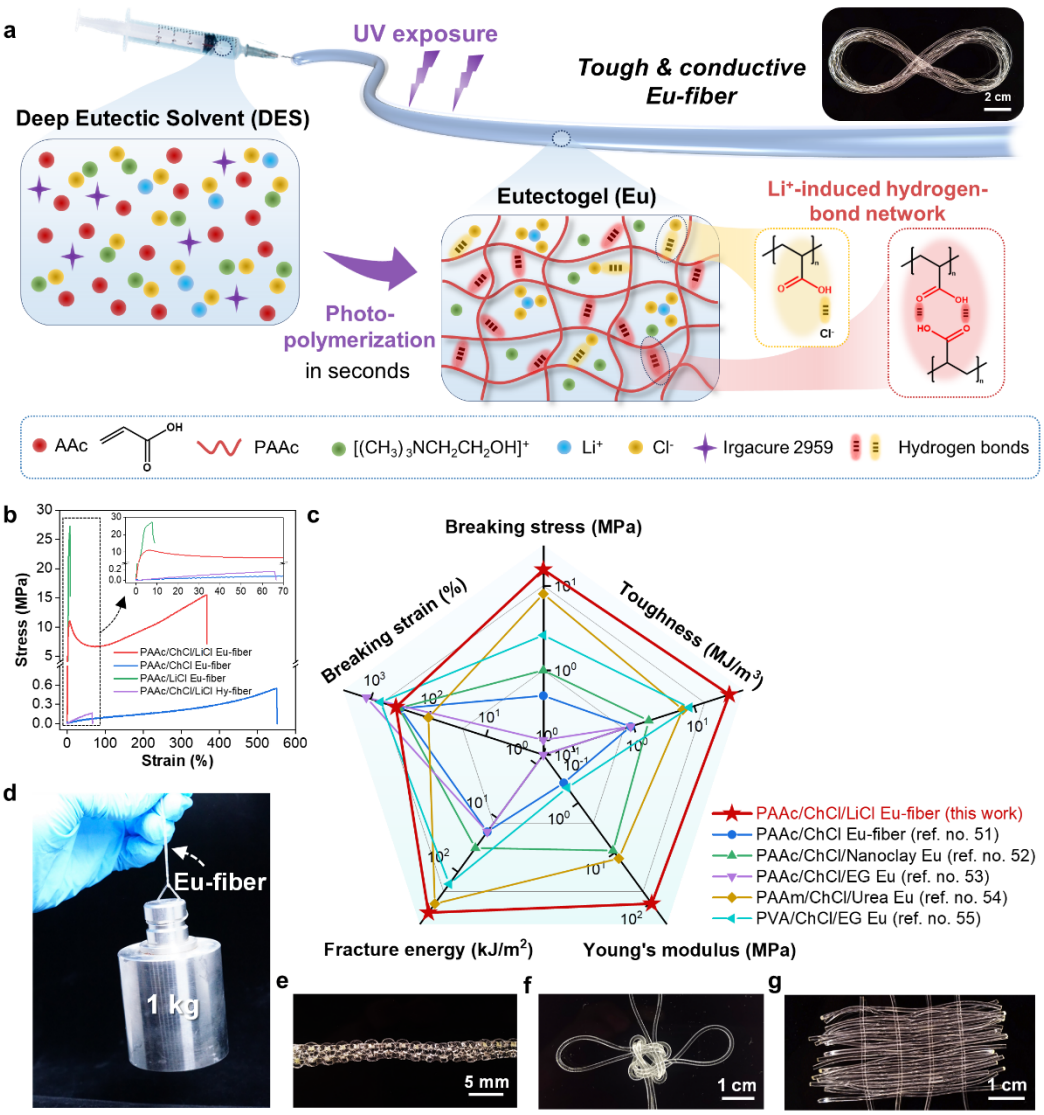

Figure 1. Design and fabrication of PAAc/ChCl/LiCl eutectogel fiber (Eu-fiber).

(a) Fabrication of PAAc/ChCl/LiCl Eu-fiber and schematic illustration of polymer network of the corresponding eutectogel. Inset shows the 2 m-long Eu-fiber fabricated in one pot (scale bar: 2 cm). (b) Comparison of tensile properties of PAAc/ChCl/LiCl Eu-fiber, PAAc/ChCl Eu-fiber, PAAc/LiCl Eu-fiber, and PAAc/ChCl/LiCl hydrogel fiber (Hy-fibers). (c) Summary of the breaking stress, Young's modulus, toughness, fracture energy and breaking strain of PAAc/ChCl/LiCl Eu-fiber, PAAc/ChCl Eu-fiber, PAAc/LiCl Eu-fiber, PAAc/ChCl/LiCl Hy-fiber (the molar ratio of AAc, ChCl, and LiCl in both eutectogel and hydrogel systems is 10:5:2) and other eutectogels reported in the literatures. (d) Digital image showing that PAAc/ChCl/LiCl Eu-fiber can lift 1 kg weight. (e-g) Digital images showing the applications of PAAc/ChCl/LiCl Eu-fibers in (e) braiding, (f) knotting, and (g) weaving.

289

290 *3.2. Mechanical properties of PAAc/ChCl/LiCl Eu-fibers*

291 The significant enhancement in the mechanical strength of eutectogels induced by Li^+ was first
292 investigated by varying the molar ratios of LiCl in the DES. To clarify the effect of the LiCl on
293 the mechanical properties of newly formed eutectogels, $PAAc_x/ChCl_y/LiCl_z$ Eu-fibers with
294 different molar ratios of LiCl and ChCl were fabricated (x, y, z are respectively the molar ratios
295 of AAc, ChCl, and LiCl). The increase of the molar ratio of ChCl in PAAc/ChCl/LiCl Eu-fibers
296 led to the increase of breaking strain but did not make significant contributions to the
297 improvement of mechanical strength (Figure S7). On the contrary, increasing the amount of
298 LiCl in the gel system demonstrated a dramatical enhancement in breaking strength and a
299 remaining high level of stretchability (>300%) (Figure 2a). As summarized in Figure 2b,
300 $PAAc_{10}/ChCl_5/LiCl_{0.5}$ Eu-fiber with only a small amount of LiCl possessed a high Young's
301 modulus of 32 MPa and toughness of 10 MJ/m^3. Further increasing the molar ratio of LiCl to
302 2 led to a significant increase in the Young's Modulus to 103 MPa and toughness to 38 MJ/m^3,
303 while the breaking strain of the $PAAc_{10}/ChCl_5/LiCl_2$ Eu-fiber was still above 360% (Figure 2b).
304 Such findings indicated that the toughening (toughness) and stiffening (Young's modulus) of
305 PAAc/ChCl/LiCl eutectogels were induced by the addition of Li salts.

306

307 The design principle of tough eutectogels in this work is to introduce additional HBA, i.e., LiCl,
308 to the AAc/ChCl DES precursor. Note that PAAc/ChCl eutectogel was formed by the
309 polymerization of AAc monomers and the inherent hydrogen bonding between ChCl and PAAc
310 network (typically between carboxylic group (-COOH) of AAc and Cl^- of ChCl),[49] we
311 believed that the introduction of Li^+ could regulate these interactions and thus led to the
312 reconstruction of the PAAc polymeric structures. To understand the hydrogen bonding
313 interactions between HBD (i.e., AAc) and HBAs (i.e., ChCl and LiCl) in DESs, and to
314 investigate the effect of LiCl on theses interactions within PAAc/ChCl/LiCl eutectogel, ^1H
315 nuclear magnetic resonance (NMR) spectroscopy was first used to evaluate the DESs and
316 eutecogels with different HBA and HBDs components. As reflected by the ^1H NMR spectrum
317 of different DESs, the addition of ChCl and LiCl into AAc led to significant proton shifts (H_a,

H_b, H_c) of AAc (Figure 2c). Since ChCl and LiCl did not display any signal within the investigated chemical shift range (5.0-8.0 ppm) (Figure S8), the proton shifts in AAc/ChCl, AAc/LiCl, and AAc/ChCl/LiCl DESs could be ascribed to the interactions between -COOH of AAc and Cl^- of ChCl/LiCl (-COOH···Cl^-). The proton shift of the ChCl in PAAc/ChCl and PAAc/ChCl/LiCl eutectogels were also investigated to reveal the effect of LiCl. The proton signal (H_d, H_e, H_f, H_g) on ChCl in the PAAc/ChCl eutectogel slightly shifted to lower fields after adding Li salts (Figure 2d). Such a chemical shift could be ascribed to the decrease of -COOH···Cl^- hydrogen bonding between PAAc and ChCl, which was caused by the addition of LiCl.

The formation of hydrogen bonding between PAAc polymer chains (O-H···O=C) hydrogen bonding in PAAc/ChCl/LiCl eutectogels with different amounts of Li^+ was then evaluated by Fourier-transform infrared spectroscopy (FTIR). Broad bands of O-H stretching vibration, which could be ascribed to different types of hydrogen bonding interactions of hydroxyl group (-OH), were observed around 3300-3400 cm^{-1} in the FTIR spectra of PAAc/ChCl and PAAc/ChCl/LiCl eutectogels (Figure 2e). Such an O-H stretching peak that was originally observed 3334 cm^{-1} in the FTIR spectrum of PAAc/ChCl eutectogel shifted from 3341 cm^{-1} to 3360 cm^{-1} as the molar ratio of LiCl in PAAc/ChCl/LiCl eutectogels increased from 1 to 2. In addition, a shoulder peak that belongs to the asymmetric vibration of C=O was observed around 1600-1800 cm^{-1}, which shifted to lower wavenumber with the amount of LiCl increased. These results confirmed that more intra- and interchain O-H···O=C hydrogen bonds between PAAc polymer chains were formed in PAAc/ChCl/LiCl eutectogel with the increase of the molar ratio of LiCl.[57, 58]

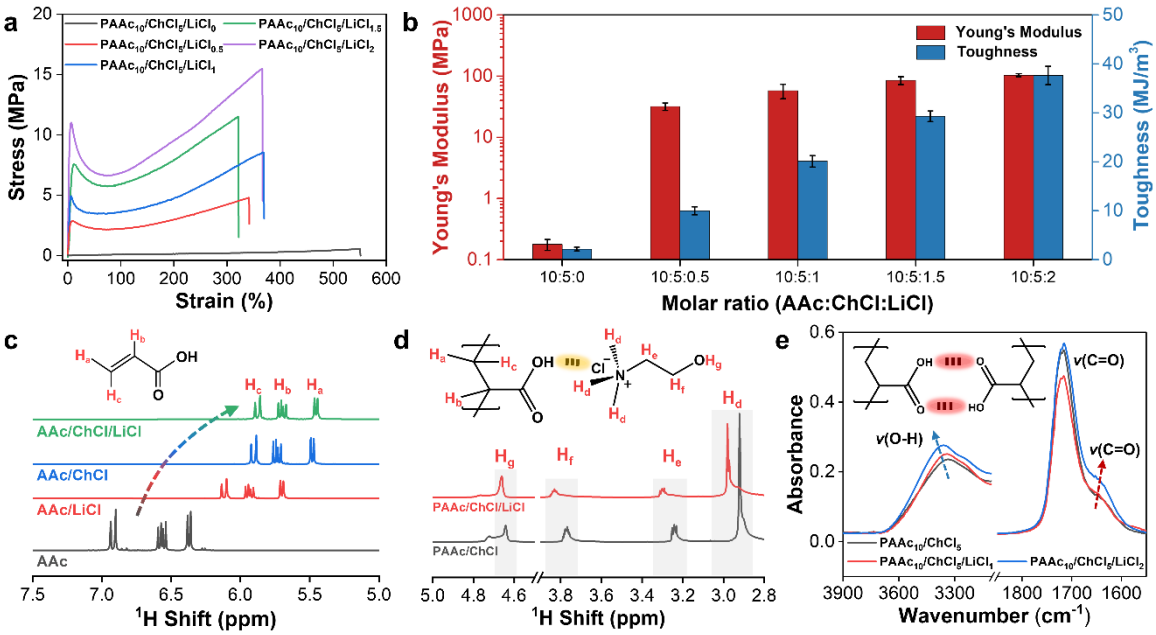

Figure 2. Mechanical properties of PAAc/ChCl/LiCl eutectogels and characterization of AAc/ChCl/LiCl DESs and PAAc/ChCl/LiCl eutectogels.

(a) Tensile stress-strain curves and (b) summary of mechanical properties of PAAc/ChCl/LiCl Eu-fibers with different molar ratios of LiCl. (c) Changes of H of AAc in ^{1}H nuclear magnetic resonance (NMR) spectra with the addition of ChCl or LiCl. (d) Comparison of ^{1}H NMR spectra of ChCl for $PAAc_{10}/ChCl_5$ eutectogel and $PAAc_{10}/ChCl_5/LiCl_1$ eutectogel. (e) FTIR spectra of eutectogels with different molar ratio of LiCl.

3.3. Toughening mechanism enabled by Li^+-induced dense hydrogen-bond network

In recent studies on the ChCl-urea DES system with LiCl salts, it emerged that the strong coordination of Li^+ with Cl^- led to the formation of $LiCl_3^{2-}$. The emergence of these negatively charged species could induce an extensive hydrogen-bond network in the ChCl-urea DES.[59] Accordingly, we speculated that such a similar situation occurred in PAAc/ChCl/LiCl eutectogel, where Li^+ had stronger coordination with Cl^- anions so that less Cl^- were around the choline cations. As such, the -COOH···Cl^- hydrogen bonding between PAAc and ChCl decreased, and PAAc tended to form interchain hydrogen bonding instead (O-H···O=C). We then applied density functional theory (DFT) calculations and molecular dynamics (MD) simulations to investigate the solvation structure of the key species in the eutectogel systems, which could further reveal the effects of Li salt on the polymeric structure of the eutectogel. As

shown in Figure 3a, Li^+, which served as monodentate coordination site (-645.32 kJ/mol), bidentate coordination site (-869.69 kJ/mol), and tridentate coordination site (-640.69 kJ/mol) with Cl^-, exhibited higher binding energy compared to the coordination of PAAc with Cl^- (-162.19 kJ/mol). Such a strong coordination ability of Li^+ with Cl^- could lead to the formation of negatively charged species ($LiCl_n^{(n-1)-}$). When the amounts of anions (i.e., Cl^-) in the eutectogel system became less, -COOH among PAAc polymer chains with the lowest binding energy (-19.43 kJ/mol) could form the interchain O-H···O=C hydrogen bonds with each other. As such, a strong PAAc network cross-linked with sufficient interchain hydrogen bonds was formed. To further investigate the effect of Li^+ on the interaction of PAAc with Cl^- (PAAc-Cl^-), molecular dynamics (MD) simulations were conducted, and the radial distribution functions g(r) were obtained (Figure 3b). In the absence of Li^+, the characteristic peaks of PAAc-Cl^- pairs appeared within the 2-6 Å range, indicating distinct binding sites of PAAc-Cl^- at different distances. Conversely, with the introduction of Li^+ additive, peaks denoting PAAc-Cl^- binding sites were not detected, suggesting a significant weakening of the union between PAAc and Cl^- upon Li^+ incorporation (Figure 3b). Also, Li^+ possessed a strong coordination ability with Cl^-, which was supported by the appearance of a sharp peak of Li^+-Cl^- with an intensity of 75 at 2.28 Å in the radial distribution function g(r). At such a distance of 2.68 Å, the coordination shell of each Li^+ ion could comprise three Cl^- ions (n(r)=3 at 2.68 Å), implying the formation of $LiCl_3^{2-}$ (Figure S9). Supported by these simulation results, the strong coordination of Li^+ with Cl^- has been proven to compete for the hydrogen bonding between PAAc polymer chains and Cl^-. When more Cl^- were bounded with Li^+, it is expected that PAAc chains were inclined to form interchain O-H···O=C hydrogen bonds rather than forming -COOH···Cl^- hydrogen bonds with free Cl^- in the system. We also calculated the effective crosslinking densities of PAAc/ChCl/LiCl Eu-fibers with different Li^+ concentrations according to classical rubber elasticity theory. The effective crosslinking densities increased remarkably from 17.8 mol/m^3 to 15.5 kmol/m^3 with the increase of the molar ratio of LiCl from 0 to 2 (Figure 3c). On this basis, this theoretical analysis supported that the addition of Li salts into PAAc/ChCl eutectogel system induced the decrease of -COOH···Cl^- hydrogen bonding of PAAc-Cl^- and the increase of O-H···O=C hydrogen-bonded crosslinks among PAAc polymer chains, which could reduce

the distance between polymer chains (Figure 3d) and thus led to the toughening of PAAc/ChCl/LiCl eutectogel.

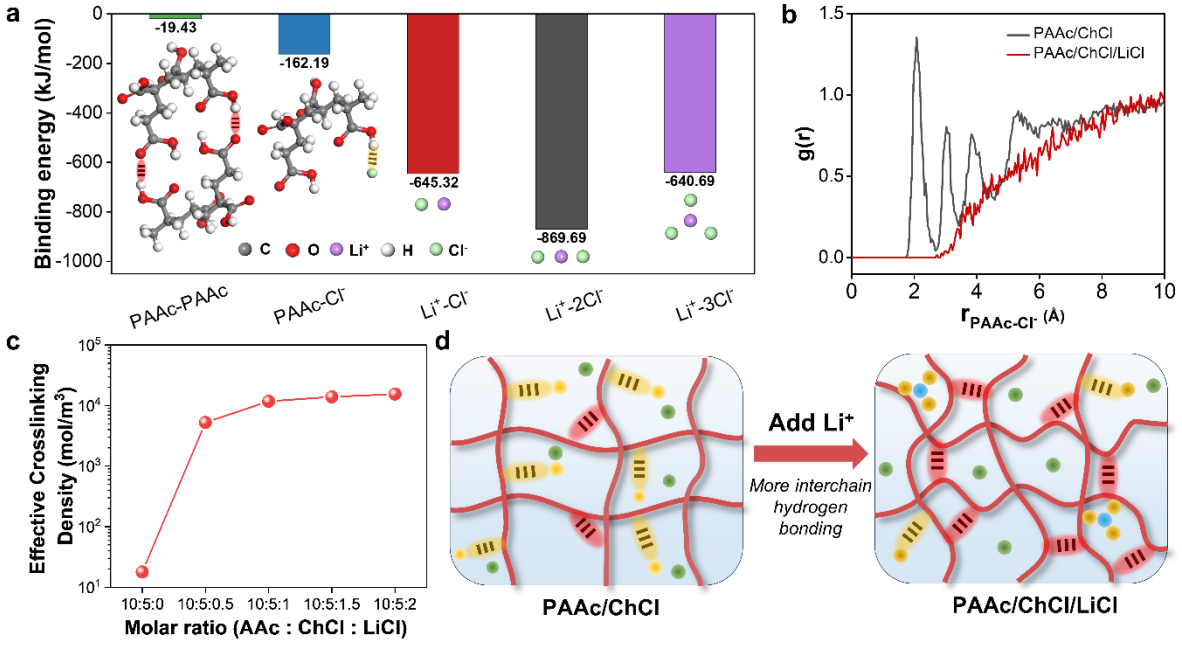

Figure 3. Simulation study of interactions in PAAc/ChCl/LiCl Eu-fiber and Li^+-induced toughening mechanism.

(a) Binding energies of different species in PAAc/ChCl/LiCl eutectogel system. Inset showing the molecular models representing binding between each components. (b) Molecular dynamics simulation showing the coordination of PAAc with Cl^- (g(r): radial distribution function). (c) Effective crosslinking densities of PAAc/ChCl/LiCl eutectogels with different molar ratio of LiCl. (d) Schematic illustration showing the effect of adding Li salts on the polymeric structure,

3.4. Versatility of Li^+-induced toughening effect

Upon the verification of the toughening mechanism of Li^+ ions, we investigated the versatility of preparing tough eutectogels by forming dense hydrogen-bonding associations with other types of Li salts. We formed three-component DESs with different Li salts, including halide Li salt (i.e., lithium bromide (LiBr)) and organic Li salts (i.e., Lithium bis(trifluoromethane sulfonyl) imide (LiTFSI) and lithium acetate (CH_3COOLi, LiOAc)) (Figure 4a), and then conducted the one-pot photopolymerization to transform these transparent liquids into the eutectogels. Though eutectogels could be formed with different Li salts, the toughening effects

varied. For example, PAAc/ChCl/LiBr eutectogel exhibited Young's modulus (38 MPa) that was comparable to PAAc/ChCl/LiCl eutectogel, which could be attributed to the similar property of Br^- as halide anion with that of Cl^- (Figure 4b). While eutectogels with LiTFSI also demonstrated promisingly strong mechanical properties, the toughening effect in the gel with LiOAc was not as obvious as that in the gel system with LiTFSI. Different from the hydrogen bonding interaction between Cl^- ions and -COOH groups, the observed enhancement of mechanical properties in the case of LiTFSI could be attributed to the establishment of a network of hydrogen bonds between the $TFSI^-$ anions and polymer chains. In this system, the hydrogen atoms within the PAAc chains (-CH) acted as donors for the hydrogen bonds, while the electronegative atoms, such as fluorine (F) and nitrogen (N) in the $TFSI^-$ anions served as the acceptors.[60, 61] However, in the case of LiOAc, it was likely that the CH_3COO^- anions competed with the inter-chain hydrogen bonding (O-H···O=C), leading to a decrease in the strength and density of cross-links within the polymeric matrix.[62] These changes in hydrogen bonding also resulted in the degradation of toughening effect as well as optical transparency (Figure 4c). Overall, such a proof-of-concept study revealed that it was applicable to utilize different Li salts to realize the toughening of the eutectogels. Further investigation on the effect of different species of anions on the physical, chemical, and mechanical properties of the eutectogels could broaden the versatility of the toughening strategies that were enabled by the Li^+-induced dense hydrogen-bond network.

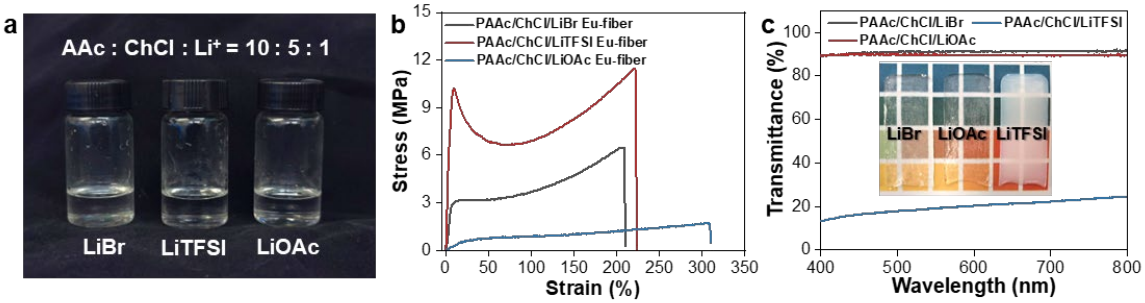

Figure 4. Versatility of Li^+-induced toughening mechanism in eutectogels with other types of Li salts.

(a) Schematic illustration showing the effect of adding Li salts on the polymeric structure. (b)

Tensile stress-strain curves of PAAc/ChCl/Li^+ Eu-fibers with different Li salts. (c) Optical transparency of PAAc/ChCl/Li^+ eutectogel with different Li salts.

3.5. Multifunction of tough Eu-fibers

Apart from the strong mechanical properties, the tough Eu-fibers also exhibited glassy-to-rubbery transition at near-body temperature, imparting the fibers with multifunction in smart shape-memory behavior. We verified that the amount of Li^+ leading to the changes in the form of hydrogen bonding could make an effect on the glass transition temperature (T_g), which could in turn tune the mechanical performance of the PAAc/ChCl/LiCl Eu-fibers in response to temperature changes. We performed dynamic mechanical analysis (DMA) and DSC to investigate the T_g of the PAAc/ChCl/LiCl eutectogels with different molar ratios of LiCl (Figure 5a and S10). The results showed that the T_g of eutectogel increased from -40 ºC to 41 ºC, which could be ascribed to the increasing interchain bonding in the polymeric network that was induced by the increasing amount of Li^+. As such, the effect of T_g could be further reflected by the changes in the tensile property of the Eu-fiber in response to the temperature changes. Under the condition of room temperature (20 ºC~30 ºC), the Eu-fiber demonstrated strong and tough mechanical properties with an obvious plastic deformation behavior at low strain (~10%). When the temperature increased from 40 ºC to 70 ºC, the Eu-fiber became softer and more elastic without showing plastic deformation. The breaking stress and Young's modulus of the Eu-fiber could respectively decrease from 14.31 MPa and 120.9 MPa at room temperature to 0.21 MPa and 0.63 MPa at 70 ºC, whereas its breaking strain increased from 245% to 1,030% (Figure 5b). Such a glassy-to-rubbery transition could be ascribed to the dissociation of hydrogen bonds between the polymer chains at the high temperature, especially above the T_g of the Eu-fiber.[63] When hydrogen bonds became weaker and less, the chain mobility increased and thus the deformation pattern of Eu-fiber changed from plastic to elastic.

Owing to this glassy-to-rubbery transition behavior, Eu-fiber could demonstrate the smart shape memory effect at the near-body temperature. For example, we programmed an Eu-fiber (dyed with 0.01 wt% Sudan I for better visualization) from a coil shape to a flat shape at 40 ºC,

and then cooled the programmed fiber at room temperature to fix the programmed flat shape. When the fiber was again heated above 37 ºC, we observed that the fiber restored its original shape (i.e., coil shape) within 30s (Figure 5c, Video S1). Such a shape-memory behavior was aroused from the temperature-dependent phase behavior of the Eu-fiber. As discussed above, PAAc/ChCl/LiCl eutectogoel exhibited the T_g around 30~40 ºC. Above T_g, the supramolecular network consisting of hydrogen bonds, was in a state of high entropy and exhibits mobility, leading to the great deformability of fiber. Upon cooling to room temperature, the hydrogen bonds were reestablished, resulting in a fixation of the shape into a temporary configuration. This process imparted strain energy into the polymer network. Upon reheating, the fiber regained mobility and allowed for molecular movements, thus releasing the stored strain energy and enabling the structure to revert back to its original state.[64] Since the shape-memory effect of Eu-fiber occurred at a temperature close to that of human body temperature, it is foreseen that Eu-fiber could be applied as temperature-sensing material for wearable temperature monitoring and fever detection.

With the existence of ChCl and LiCl in the gels, the Eu-fiber exhibited a promising ionic conductivity. PAAc/ChCl/LiCl Eu-fiber exhibited ionic conductivity ranging from 4×10^{-3} S/m to 6×10^{-3} S/m with the different molar ratios of LiCl (Figure 5d). They also exhibited excellent dehydration properties and good stability at a relative humidity of 40% due to their solvent-free nature. The mechanical properties and ionic conductivities of Eu-fibers during a storage period of 7 days at a temperature of 25 ºC and relative humidity of 40% were investigated. During the storage period, the fibers reached an equilibrium state and absorbed water equivalent to 12% of their own weight. Figure S11 illustrates the observed changes, with Young's modulus decreasing from 57.93 MPa to 13.57 MPa, the ionic conductivities increasing from 6×10^{-3} to 3.1×10^{-2} S/m. The subtle fluctuations observed in the mechanical and conductive properties offered compelling evidence regarding the robust and enduring performance stability of Eu-fibers following extended storage periods. Moreover, the resistance change of the gel fiber was highly dependent on the stretching strain particularly at high temperature conditions. Herein, we used $(R-R_0)/R_0$ to define the relative resistance change of

493 the Eu-fiber in response to the strain change, where R_0 was the resistance of the fiber at the
494 pristine status (at 0% strain) and R was the resistance measured under stretch. The $(R-R_0)/R_0$
495 value of the Eu-fiber increased with the increasing strain and demonstrated a high linearity and
496 a good reversibility in the stretching range of 0~300% (Figure 5e and f, Figure S12a).
497 Furthermore, the Eu-fibers exhibited stable strain sensing performance during 4000 s at a 100%
498 strain (Figure S12b). The reason for these resistance changes upon stretching could be
499 attributed to the deformation of the polymeric network of the Eu-fiber in the tensile direction
500 during the stretching process, which led to changes in the ion conduction path and the increase
501 in the resistance of the fiber. Such a strain-dependent electrical property endows the Eu-fiber
502 with the capability of a strain sensor and excellent stability at high temperature for applications
503 of wearable motion detection.
504
505 More importantly, owing to large amounts of reversible non-covalent crosslinks in the
506 polymeric network, eutectogel could be fully dissolved into water with the dissociation of
507 hydrogen bonds and then reformed into a gel by the reconstruction of the bonding in the
508 polymeric network. As a proof of concept, we dissolved a batch of Eu-fiber (dyed with 0.01
509 wt% Sudan I for better visualization) into a bath of hot water to form an aqueous solution of
510 PAAc/ChCl/LiCl, and then ejected the solution into a mold to re-form a dumbbell-shaped gel
511 film (Figure 5g). Especially, the mechanical and electrical property of the recycled eutectogel
512 was similar to that of the Eu-fiber before recycling (Figure 5h). The electrical conductivity of
513 the recycled eutectogel was around 5.1 x 10^{-2} S/m according to the equation $\sigma = L/RS$, where
514 R was measured by an LCR meter. The value closely aligned with the electrical conductivity
515 of the original Eu-fiber, which stood at approximately 4.8 x 10^{-2} S/m. For safety and
516 environmental considerations, the commendable recyclability of Eu-fibers held promise for
517 facilitating the reutilization of Li salts. Notably, the complete dissolution of eutectogels into
518 water with the dissociation of hydrogen bonds allowed for the recycling of disabled or damaged
519 eutectogels in the production of fresh ones. This also enabled the separation and refinement of
520 Li salts via chemical processes. Therefore, Eu-fiber could be recycled to reduce the waste of
521 materials recourses, particularly in addressing the adverse impact of Li^+ disposal on safety and

the environment, which could greatly benefit the sustainability of green chemistry.

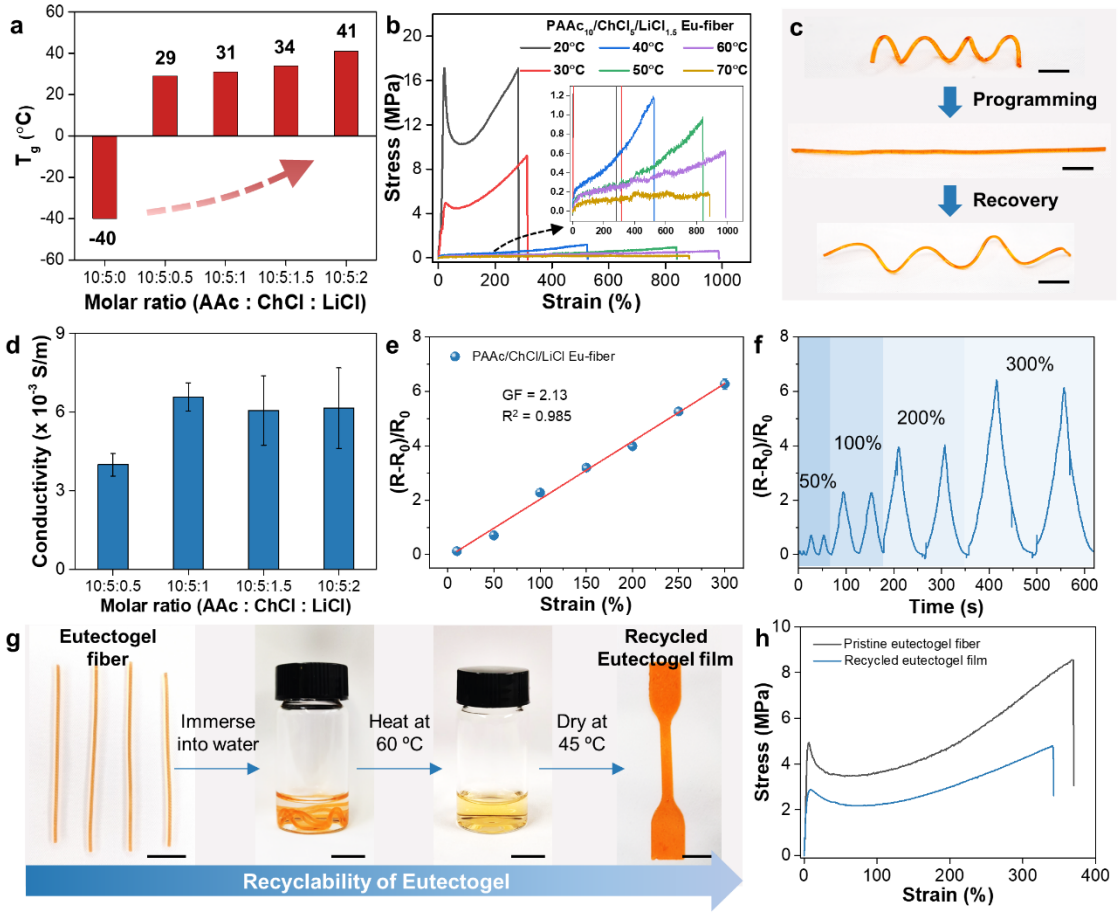

Figure 5. Eu-fibers with multifunction in shape memory behavior, strain sensing, and recyclability.

(a) Glass transition temperatures (T_g) of PAAc/ChCl/LiCl eutectogels with different molar ratios of LiCl. (b) Tensile stress-strain curves of $PAAc_{10}/ChCl_5/LiCl_{1.5}$ Eu-fiber measured at different temperatures. (c) Digital images showing the shape recovery process of Eu-fibers that restored from the programmed shape to its original coil shapes (Eu-fiber was dyed with 0.01 wt% Sudan I for better visualization) (Scale bar: 1cm). (d) Ionic conductivity of PAAc/ChCl/LiCl eutectogel synthesized with different molar ratios of LiCl. (e) Relative resistance changes of Eu-fiber under different stretching strains at 50 °C. (f) Relative resistance changes of Eu-fiber for 50%, 100%, 200%, and 300% strain at 50 °C. (g) Recyclability of eutectogel (Eu-fiber was dyed with 0.01 wt% Sudan I for better visualization) (Scale bar: 1 cm). (h) Tensile stress-strain curves of pristine Eu-fiber and the recycled eutectogel film.

4. Conclusion

In summary, this work demonstrates a simple and versatile spinning approach based on one-pot photopolymerization and Li^+-induced toughening effect to fabricate super-strong and conductive Eu-fibers toughen with dense hydrogen-bond networks. The obtained Eu-fibers exhibit superb breaking strength (15.5 MPa), Young's modulus (103.8 MPa), toughness (38 MJ/m^3) with promising stretchability (>300%). Such super-strong mechanical properties can be attributed to the superior coordination of Li^+ with Cl^- that leads to the formation of negatively charged ion pairs ($LiCl_n^{(n-1)-}$). As a result, when there are fewer free Cl^- anions in the polymer matrix, -COOH groups of PAAc tend to form stronger interchain hydrogen bonds rather than forming hydrogen bonds with Cl^-. Moreover, the utilization of DESs endows the Eu-fibers with good temperature tolerance and conductivity ($4\sim6 \times 10^{-3}$ S/m), making it perform as a promising candidate to flexible ionic conductors for strain sensing applications. In addition, the newly developed eutectogel demonstrates the shape memory behavior near the human body temperature, which can allow for the application as temperature-sensitive materials in temperature monitoring and fever detection. Owning to the reversible hydrogen bonds in the conformation of the polymeric network, such type of eutectogel can be recycled, so that waste of materials resources can be effectively avoided. Further exploration of the materials combination for DESs and eutectogel and the engineering of the fiber processing could greatly benefit the materials library for these new types of ionic gel fibers, and thus promote the development of robust and multifunctional smart materials for the next-generation soft electronics.

Author contribution

L.F., W.G. and Q.H. conceived and designed the experiments. L.F., M.R., F.C and Z.C. performed the experiments. L.F., W.G. and Q.H. analyzed the data. C.Z. conducted the simulation studies. L.F. and Q.H. wrote the manuscript. X.W., Z.Z. and Q.H. reviewed and edited the manuscript. All authors discussed the results and commented on the manuscript.

Declaration of Competing Interest

The authors declare that they have no known competing financial interests or personal relationships that could have appeared to influence the work reported in this paper.

Acknowledgments

This work was supported by the General Research Fund of Hong Kong (15212021), Shenzhen Science and Technology Innovation Committee (SGDX20210823103403033), RI-Wear Seed Fund of PolyU (1-CD8D), Start-up Fund of PolyU (1-ZVT8), and NSFC's Young Scientists Fund (52203318). The authors also thank the technical support from University Research Facility in Chemical and Environmental Analysis (UCEA) and University Research Facility in Materials Characterization and Device Fabrication (UMF).

References

[1] W. Kong, C. Wang, C. Jia, Y. Kuang, G. Pastel, C. Chen, G. Chen, S. He, H. Huang, J. Zhang, Muscle-inspired highly anisotropic, strong, ion-conductive hydrogels, Advanced Materials 30(39) (2018) 1801934.

[2] Y. Zhou, C. Wan, Y. Yang, H. Yang, S. Wang, Z. Dai, K. Ji, H. Jiang, X. Chen, Y. Long, Highly stretchable, elastic, and ionic conductive hydrogel for artificial soft electronics, Advanced Functional Materials 29(1) (2019) 1806220.

[3] D. Ji, J.M. Park, M.S. Oh, T.L. Nguyen, H. Shin, J.S. Kim, D. Kim, H.S. Park, J. Kim, Superstrong, superstiff, and conductive alginate hydrogels, Nature Communications 13(1) (2022) 1-10.

[4] J. Song, S. Chen, L. Sun, Y. Guo, L. Zhang, S. Wang, H. Xuan, Q. Guan, Z. You, Mechanically and electronically robust transparent organohydrogel fibers, Advanced Materials 32(8) (2020) 1906994.

[5] Y. Ding, J. Zhang, L. Chang, X. Zhang, H. Liu, L. Jiang, Preparation of high-performance ionogels with excellent transparency, good mechanical strength, and high conductivity, Advanced Materials 29(47) (2017) 1704253.

[6] F. Mo, G. Liang, D. Wang, Z. Tang, H. Li, C. Zhi, Biomimetic organohydrogel electrolytes for high-environmental adaptive energy storage devices, EcoMat 1(1) (2019) e12008.

[7] C. Keplinger, J.-Y. Sun, C.C. Foo, P. Rothemund, G.M. Whitesides, Z. Suo, Stretchable, transparent, ionic conductors, Science 341(6149) (2013) 984-987.

[8] S. Lin, H. Yuk, T. Zhang, G.A. Parada, H. Koo, C. Yu, X. Zhao, Stretchable hydrogel electronics and devices, Advanced Materials 28(22) (2016) 4497-4505.

[9] H. Yuk, B. Lu, X. Zhao, Hydrogel bioelectronics, Chemical Society Reviews 48(6) (2019) 1642-1667.

[10] X. Liu, J. Liu, S. Lin, X. Zhao, Hydrogel machines, Materials Today 36 (2020) 102-124.

[11] S. Zhang, Z. Xia, Z. Liu, Q. Wang, Y. Yue, J. Huang, B. Su, Magnetic/conductive/elastic

multi-material 3D-printed self-powered sensing gloves for underwater/smoke environmental Human-Computer Interaction, Chemical Engineering Journal 463 (2023) 142388.
[12] Y. Dobashi, D. Yao, Y. Petel, T.N. Nguyen, M.S. Sarwar, Y. Thabet, C.L. Ng, E. Scabeni Glitz, G.T.M. Nguyen, C. Plesse, Piezoionic mechanoreceptors: Force-induced current generation in hydrogels, Science 376(6592) (2022) 502-507.
[13] Y. Li, Z. Li, Q. Wang, Z. Wu, C. Shi, S. Zhang, Y. Xu, X. Chen, A. Chen, C. Yan, 3D-printed magnetic porous structures with different poisson's ratios and their mechanoelectrical conversion capabilities, Additive Manufacturing 69 (2023) 103542.
[14] Y. Lee, W. Song, J.-Y. Sun, Hydrogel soft robotics, Materials Today Physics 15 (2020) 100258.
[15] B. Yiming, X. Guo, N. Ali, N. Zhang, X. Zhang, Z. Han, Y. Lu, Z. Wu, X. Fan, Z. Jia, Ambiently and mechanically stable ionogels for soft ionotronics, Advanced Functional Materials 31(33) (2021) 2102773.
[16] G. Li, Z. Deng, M. Cai, K. Huang, M. Guo, P. Zhang, X. Hou, Y. Zhang, Y. Wang, Y. Wang, A stretchable and adhesive ionic conductor based on polyacrylic acid and deep eutectic solvents, npj Flexible Electronics 5(1) (2021) 1-8.
[17] C. Zhao, L. Chen, Y. Ru, L. Zhang, M. Liu, Thermoresponsive ionogels with switchable adhesion in air and aqueous environments induced by LCST phase behavior, Soft Matter 18(32) (2022) 5934-5938.
[18] S. Wu, Y. Alsaid, B. Yao, Y. Yan, Y. Zhao, M. Hua, D. Wu, X. Zhu, X. He, Rapid and scalable fabrication of ultra-stretchable, anti-freezing conductive gels by cononsolvency effect, EcoMat 3(2) (2021) e12085.
[19] F. Chen, D. Zhou, J. Wang, T. Li, X. Zhou, T. Gan, S. Handschuh-Wang, X. Zhou, Rational fabrication of anti-freezing, non-drying tough organohydrogels by one-pot solvent displacement, Angewandte Chemie 130(22) (2018) 6678-6681.
[20] A.P. Abbott, G. Capper, D.L. Davies, R.K. Rasheed, V. Tambyrajah, Novel solvent properties of choline chloride/urea mixtures, Chemical communications (1) (2003) 70-71.
[21] B.B. Hansen, S. Spittle, B. Chen, D. Poe, Y. Zhang, J.M. Klein, A. Horton, L. Adhikari, T. Zelovich, B.W. Doherty, Deep eutectic solvents: A review of fundamentals and applications, Chemical reviews 121(3) (2020) 1232-1285.
[22] C. Zhang, L. Zhang, Y. Ding, X. Guo, G. Yu, Eutectic electrolytes for high-energy-density redox flow batteries, ACS Energy Letters 3(12) (2018) 2875-2883.
[23] J.D. Mota-Morales, E. Morales-Narváez, Transforming nature into the next generation of bio-based flexible devices: New avenues using deep eutectic systems, Matter 4(7) (2021) 2141-2162.
[24] W. Cheng, Y. Liu, Z. Tong, Y. Zhu, K. Cao, W. Chen, D. Zhao, H. Yu, Micro-interfacial polymerization of porous PEDOT for printable electronic devices, EcoMat 5(2) (2023) e12288.
[25] Y. Wan, S. Huang, Y. Sun, H. Zhu, Q. Zheng, Q. Zhang, S. Zhu, Superstrong yet water-detachable eutectogel adhesives, Chemical Engineering Journal 442 (2022) 136289.
[26] H. Sun, B. Zhang, L. Lu, Z. Chen, Y. Huo, W. Li, B. Zhang, J. Song, d-gluconic acetal gelator-based supramolecular–Polymer dual network eutectogels for high performance temperature, strain, and pressure sensors, Chemical Engineering Journal 451 (2023) 139051.
[27] Z. Ma, Q. Wang, Z. Wu, D. Chen, C. Yan, Y. Shi, M.D. Dickey, B. Su, A Superconducting-Material-Based Maglev Generator Used for Outer-Space, Advanced Materials 34(33) (2022)

2203814.
[28] J. Lan, B. Zhou, C. Yin, L. Weng, W. Ni, L.-Y. Shi, Zwitterionic dual-network strategy for highly stretchable and transparent ionic conductor, Polymer 231 (2021) 124111.
[29] S. Hong, Y. Yuan, C. Liu, W. Chen, L. Chen, H. Lian, H. Liimatainen, A stretchable and compressible ion gel based on a deep eutectic solvent applied as a strain sensor and electrolyte for supercapacitors, Journal of Materials Chemistry C 8(2) (2020) 550-560.
[30] H. Qin, R.E. Owyeung, S.R. Sonkusale, M.J. Panzer, Highly stretchable and nonvolatile gelatin-supported deep eutectic solvent gel electrolyte-based ionic skins for strain and pressure sensing, Journal of Materials Chemistry C 7(3) (2019) 601-608.
[31] H. Yang, J. Zhang, J. Yao, D. Zuo, J. Xu, H. Zhang, A gel polymer electrolyte based on ternary deep eutectic solvent for flexible, wide-temperature tolerant zinc-ion hybrid supercapacitors, Journal of Power Sources 548 (2022) 232070.
[32] H. Yang, M. Sang, G. Li, D. Zuo, J. Xu, H. Zhang, Stretchable, self-healable, conductive and adhesive gel polymer electrolytes based on a deep eutectic solvent for all-climate flexible electrical double-layer capacitors, Journal of Energy Storage 45 (2022) 103766.
[33] M. Wang, J. Hu, M.D. Dickey, Tough Ionogels: Synthesis, Toughening Mechanisms, and Mechanical Properties-A Perspective, JACS Au 2(12) (2022) 2645-2657.
[34] K. Fan, W. Wei, Z. Zhang, B. Liu, W. Feng, Y. Ma, X. Zhang, Highly stretchable, self-healing, and adhesive polymeric eutectogel enabled by hydrogen-bond networks for wearable strain sensor, Chemical Engineering Journal 449 (2022) 137878.
[35] H. Zhang, N. Tang, X. Yu, M.H. Li, J. Hu, Strong and Tough Physical Eutectogels Regulated by the Spatiotemporal Expression of Non-Covalent Interactions, Advanced Functional Materials 32(41) (2022) 2206305.
[36] K. Zhao, K. Zhang, P. Sang, H. Hu, M. He, A very mechanically strong and stretchable liquid-free double-network ionic conductor, Journal of Materials Chemistry A 9(41) (2021) 23714-23721.
[37] Q. Huang, Z. Zheng, Pathway to developing permeable electronics, ACS nano 16(10) (2022) 15537-15544.
[38] K. Fan, L. Wang, W. Wei, F. Wen, Y. Xu, X. Zhang, X. Guan, Multifunctional self-healing eutectogels induced by supramolecular assembly for smart conductive materials, interface lubrication and dye adsorption, Chemical Engineering Journal 441 (2022) 136026.
[39] X. Wang, G. Chen, K. Zhang, R.a. Li, Z. Jiang, H. Zhou, J. Gan, M. He, Self-Healing Multimodal Flexible Optoelectronic Fiber Sensors, Chemistry of Materials 35(3) (2023) 1345-1354.
[40] F.T. Wall, Principles of Polymer Chemistry. Paul J. Flory. Cornell Univ. Press, Ithaca, New York, 1953. 688 pp. Illus. $8.50, Science 119(3095) (1954) 555-556.
[41] Y. Zhao, D.G. Truhlar, The M06 suite of density functionals for main group thermochemistry, thermochemical kinetics, noncovalent interactions, excited states, and transition elements: two new functionals and systematic testing of four M06-class functionals and 12 other functionals, Theoretical chemistry accounts 120 (2008) 215-241.
[42] F. Weigend, R. Ahlrichs, Balanced basis sets of split valence, triple zeta valence and quadruple zeta valence quality for H to Rn: Design and assessment of accuracy, Physical Chemistry Chemical Physics 7(18) (2005) 3297-3305.
[43] F. Weigend, F. Furche, R. Ahlrichs, Gaussian basis sets of quadruple zeta valence quality

692 for atoms H-Kr, The Journal of chemical physics 119(24) (2003) 12753-12762.
693 [44] S. Grimme, J. Antony, S. Ehrlich, H. Krieg, A consistent and accurate ab initio
694 parametrization of density functional dispersion correction (DFT-D) for the 94 elements H-Pu,
695 The Journal of chemical physics 132(15) (2010) 154104.
696 [45] A.P. Thompson, H.M. Aktulga, R. Berger, D.S. Bolintineanu, W.M. Brown, P.S. Crozier,
697 P.J. in't Veld, A. Kohlmeyer, S.G. Moore, T.D. Nguyen, LAMMPS-a flexible simulation tool
698 for particle-based materials modeling at the atomic, meso, and continuum scales, Computer
699 Physics Communications 271 (2022) 108171.
700 [46] H. Sun, COMPASS: an ab initio force-field optimized for condensed-phase applications
701 overview with details on alkane and benzene compounds, The Journal of Physical Chemistry
702 B 102(38) (1998) 7338-7364.
703 [47] W. Humphrey, A. Dalke, K. Schulten, VMD: visual molecular dynamics, Journal of
704 molecular graphics 14(1) (1996) 33-38.
705 [48] B.B. Hansen, S. Spittle, B. Chen, D. Poe, Y. Zhang, J.M. Klein, A. Horton, L. Adhikari, T.
706 Zelovich, B.W. Doherty, B. Gurkan, E.J. Maginn, A. Ragauskas, M. Dadmun, T.A.
707 Zawodzinski, G.A. Baker, M.E. Tuckerman, R.F. Savinell, J.R. Sangoro, Deep Eutectic
708 Solvents: A Review of Fundamentals and Applications, Chemical Reviews 121(3) (2021)
709 1232-1285.
710 [49] A.P. Abbott, D. Boothby, G. Capper, D.L. Davies, R.K. Rasheed, Deep eutectic solvents
711 formed between choline chloride and carboxylic acids: versatile alternatives to ionic liquids,
712 Journal of the American Chemical Society 126(29) (2004) 9142-9147.
713 [50] H. Qin, X. Hu, J. Wang, H. Cheng, L. Chen, Z. Qi, Overview of acidic deep eutectic
714 solvents on synthesis, properties and applications, Green Energy & Environment 5(1) (2020)
715 8-21.
716 [51] X. Wang, G. Chen, L. Cai, R.a. Li, M. He, Weavable transparent conductive fibers with
717 harsh environment tolerance, ACS Applied Materials & Interfaces 13(7) (2021) 8952-8959.
718 [52] C. Zhang, H. Zheng, J. Sun, Y. Zhou, W. Xu, Y. Dai, J. Mo, Z. Wang, 3D Printed, Solid-
719 State Conductive Ionoelastomer as a Generic Building Block for Tactile Applications,
720 Advanced Materials 34(2) (2022) 2105996.
721 [53] G. Li, Z. Deng, M. Cai, K. Huang, M. Guo, P. Zhang, X. Hou, Y. Zhang, Y. Wang, Y. Wang,
722 A stretchable and adhesive ionic conductor based on polyacrylic acid and deep eutectic solvents,
723 npj Flexible Electronics 5(1) (2021) 23.
724 [54] Q. Zhou, L. Dong, J. Wu, Y. Shi, X. Feng, X. Lu, J. Zhu, L. Mu, Versatile ionic gel driven
725 by dual hydrogen bond networks: toward advanced lubrication and self-healing, ACS Applied
726 Polymer Materials 3(11) (2021) 5932-5941.
727 [55] Y. Wang, J. Wang, Z. Ma, L. Yan, A highly conductive, self-recoverable, and strong
728 eutectogel of a deep eutectic solvent with polymer crystalline domain regulation, ACS Applied
729 Materials & Interfaces 13(45) (2021) 54409-54416.
730 [56] S. Xu, Z. Zhou, Z. Liu, P. Sharma, Concurrent stiffening and softening in hydrogels under
731 dehydration, Science Advances 9(1) (2023) eade3240.
732 [57] X. Zhang, W. Liu, D. Yang, X. Qiu, Biomimetic supertough and strong biodegradable
733 polymeric materials with improved thermal properties and excellent UV-blocking performance,
734 Advanced Functional Materials 29(4) (2019) 1806912.
735 [58] S. Selvasekarapandian, R. Baskaran, O. Kamishima, J. Kawamura, T. Hattori, Laser

Raman and FTIR studies on Li^+ interaction in PVAc-$LiClO_4$ polymer electrolytes, Spectrochimica Acta Part A: Molecular and Biomolecular Spectroscopy 65(5) (2006) 1234-1240.
[59] M.E. Di Pietro, K. Goloviznina, A. van den Bruinhorst, G. de Araujo Lima e Souza, M. Costa Gomes, A.A. Padua, A. Mele, Lithium Salt Effects on the Liquid Structure of Choline Chloride-Urea Deep Eutectic Solvent, ACS Sustainable Chemistry & Engineering 10(36) (2022) 11835-11845.
[60] B. Yiming, Y. Han, Z. Han, X. Zhang, Y. Li, W. Lian, M. Zhang, J. Yin, T. Sun, Z. Wu, A mechanically robust and versatile liquid-free ionic conductive elastomer, Advanced Materials 33(11) (2021) 2006111.
[61] P. Shi, Y. Wang, K. Wan, C. Zhang, T. Liu, A waterproof ion-conducting fluorinated elastomer with 6000% stretchability, superior ionic conductivity, and harsh environment tolerance, Advanced Functional Materials 32(22) (2022) 2112293.
[62] C. Schatz, C. Viton, T. Delair, C. Pichot, A. Domard, Typical physicochemical behaviors of chitosan in aqueous solution, Biomacromolecules 4(3) (2003) 641-648.
[63] D.J. Skrovanek, S.E. Howe, P.C. Painter, M.M. Coleman, Hydrogen bonding in polymers: infrared temperature studies of an amorphous polyamide, Macromolecules 18(9) (1985) 1676-1683.
[64] H. Guo, R. Puttreddy, T. Salminen, A. Lends, K. Jaudzems, H. Zeng, A. Priimagi, Halogen-bonded shape memory polymers, Nature Communications 13(1) (2022) 7436.